

Evidence for small-scale mantle convection in the upper mantle beneath the Baikal rift zone

Stephen S. Gao and Kelly H. Liu

Department of Geology, Kansas State University, Manhattan, Kansas, USA

Paul M. Davis and Phillip D. Slack

Department of Earth and Space Sciences, University of California, Los Angeles, California, USA

Yuliy A. Zorin, Valentina V. Mordvinova, and Vladimir M. Kozhevnikov

Institute of the Earth's Crust, Siberian Branch of Russian Academy of Sciences, Irkutsk, Russia

Received 18 June 2002; revised 2 October 2002; accepted 28 January 2003; published XX Month 2003.

[1] Inversion of teleseismic P wave travel time residuals collected along a 1280-km-long profile traversing the Baikal rift zone (BRZ) reveals the existence of an upwarped lithosphere/asthenosphere interface, which causes a travel time delay of about 1 s at the rift axis (“central high”). An area with early arrivals relative to the stable Siberian platform of up to 0.5 s is observed on each side of the rift, about 200 km from the rift axis (“flank lows”). While the location of the central high is approximately fixed in the vicinity of the rift axis, those of the flank lows vary as much as 200 km with the azimuth of the arriving rays. We use three techniques to invert the travel time residuals for velocity anomalies beneath the profile. Two of the techniques assume an isotropic velocity structure, and one of them considers a transversely isotropic velocity model with a vertical axis of symmetry. We use independent geophysical observations such as gravity, active source seismic exploration, and crustal thickness measurements to compare the applicability of the models. Other types of geophysical measurements suggest that the model involving transverse isotropy is a plausible one, which suggests that the central high and flank lows are caused by the combined effects of an upwarped asthenosphere with a 2.5% lateral velocity reduction, and a velocity increase due to transverse isotropy with a vertical axis of symmetry. We consider the anisotropy to be the result of the vertical component of a lithosphere/asthenosphere small-scale mantle convection system that is associated with the rifting.

INDEX TERMS: 7218 Seismology: Lithosphere and upper mantle; 7203 Seismology: Body wave propagation; 8109 Tectonophysics: Continental tectonics—extensional (0905); 8120 Tectonophysics: Dynamics of lithosphere and mantle—general; **KEYWORDS:** Baikal rift, tomography, anisotropy, lithosphere, asthenosphere

Citation: Gao, S. S., K. H. Liu, P. M. Davis, P. D. Slack, Y. A. Zorin, V. V. Mordvinova, and V. M. Kozhevnikov, Evidence for small-scale mantle convection in the upper mantle beneath the Baikal rift zone, *J. Geophys. Res.*, 108(0), XXXX, doi:10.1029/2002JB002039, 2003.

1. Introduction

[2] A continental rift is a region where the lithosphere is extending and is usually marked by a rift valley. Continental rifting is the first stage in a Wilson cycle, although some rifts never evolve into an oceanic basin [e.g., *Turcotte and Schubert*, 1982]. Consequently, the seismic velocity and thermal structures beneath a continental rift show a remarkable resemblance to those of an oceanic rift [*Bjarnason et al.*, 1996].

[3] The mechanisms of continental rifting can be separated into two end-members called passive and active rifting. Passive rifting is the result of extensional or shearing

stresses that originate beyond the vicinity of the resulting rift (see, e.g., *Tapponnier and Molnar* [1979] for the Baikal rift zone (BRZ)), and active rifting is the result of active intrusion of an asthenospheric diapir (see, e.g., *Turcotte and Emerman* [1983], *Logatchev and Zorin* [1992], and *Gao et al.* [1994a] for BRZ). Geodynamic modeling has been used to suggest that a small-scale mantle convection system would develop beneath a rift formed by either mechanism [*Turcotte and Emerman*, 1983; *Steckler*, 1985; *Anderson*, 1994; *King and Anderson*, 1995, 1998; *Huisman et al.*, 2001]. Major continental rifts often form at the edge of cratons in regions that have undergone transpressional tectonics in the past. It has been suggested that the associated juxtaposition of cold cratonic and warm orogenic lithosphere would cause small-scale convection in the mantle, and the subsequent rifting could lead to formation

of flood basalts [Anderson, 1994; King and Anderson, 1995, 1998]. Recently, Huismans *et al.* [2001] calculated how passive extension can destabilize the mantle lithosphere resulting in upward doming of the asthenosphere and adjacent down warping of the lithosphere into the asthenosphere. Such models can be tested using teleseismic tomography. Because the finite strains associated with the convection are expected to generate seismic anisotropy in the mantle from lattice preferred orientation (LPO) of olivine crystals (see, e.g., Blackman *et al.* [1996] for mid-ocean ridge flows), modification of the traditional isotropic tomographic inversions to include anisotropy is required. In this paper, we analyze teleseismic *P* wave travel time residuals obtained across the Baikal rift and compare isotropic and anisotropic tomographic inversions with the structures expected from small-scale convection. We conclude that small-scale convection probably exists beneath the rift and has given rise to anisotropic structure in the underlying asthenosphere.

2. Baikal Rift Zone

[4] The Baikal rift zone in Siberia is a major continental rift zone. The 1500-km-long en echelon system of rift depressions, which originated about 30 Ma along the Paleozoic suture between the Siberian and Amurian microplates, is the most seismically active continental rift in the world (Figure 1). Previous studies revealed that it has all the common features of a typical continental rift. These features [e.g., Turcotte and Schubert, 1982] include (1) a subsided central valley and uplifted adjacent blocks; (2) flanking normal faults; (3) negative Bouguer gravity anomalies [Zorin *et al.*, 1989]; (4) higher than normal heat flow [Lysak, 1984]; and (5) shallow, tensional and higher than normal seismicity [Doser, 1991]. Another feature of most continental rifts is the thinning of the crust beneath the rift valley [Davis, 1991]. Deep seismic sounding experiments reveal that beneath the BRZ, the thinning is no more than 5 km [Puzyrev, 1993], which is significantly smaller than that beneath other major rifts. A recent study from stacking of teleseismic receiver functions [Zachary *et al.*, 2000] reveals a dramatic change in Moho depth, from about 37 km beneath the Siberian Craton to about 45 km beneath the fold belt south of the rift. The change takes place over a distance of less than 20 km. The measurements suggest that the Baikal rift zone was formed near this zone of sudden change in Moho depth, which, along with a change in lithospheric thickness and age, is probably a zone of weakness.

[5] Over the last 30 years, the deep-seated structure beneath the Baikal rift zone and its adjacent regions has been studied by using various geophysical techniques, such as deep seismic sounding [Puzyrev *et al.*, 1978], gravimetric investigations [Zorin *et al.*, 1989], modeling of heat flow [Lysak, 1984, 1987; Zorin and Osokina, 1984; Zorin and Lepina, 1985], seismic spectral ratio methods [Mordvinova, 1983, 1988], magnetotelluric measurements [Popov, 1990], teleseismic travel time tomography [Gao *et al.*, 1994b; Gao, 1995], and shear wave splitting [Gao *et al.*, 1994a, 1997, 1999].

[6] Gravity and seismic studies suggest that the lithospheric thickness beneath the rift zone is about 40–50 km; beneath the Siberian platform it increases to 200 km; and in

the Mongolian foldbelt it ranges from 75 to 160–175 km [Zorin *et al.*, 1989; Logatchev and Zorin, 1992; Egorkin *et al.*, 1984]. Magnetotelluric experiments indicate that in the southern part of the Baikal rift zone, the depth of a mantle conductive layer, which was inferred to be the asthenosphere, was found to be at about 110 km depth [Popov, 1990; Kiselev and Popov, 1992]. Using teleseismic data recorded along an E-W profile across the central part of Lake Baikal, Gao *et al.* [1994b] suggest that the asthenospheric upwarp has an asymmetric shape with the NW edge being steeper. They also find that at a distance of about 300 km NW of the rift axis, the thickness of the lithosphere beneath the Siberian platform is about 100 km thick and appears to be continuously increasing at the end of the profile.

[7] Results from these previous studies provide the starting model and constraints for our travel time inversions, which are aimed at refining the velocity structure model beneath the BRZ and adjacent areas using a unique seismic data set from a profile that extended from the center of the Siberian craton across Lake Baikal to the Gobi Desert in southern Mongolia (Figure 1).

[8] Currently there is a debate on the extent of thermal modification of the rifted lithosphere beneath Lake Baikal. A broad asymmetrical region of low Bouguer gravity extending well beyond the boundaries of the lake was interpreted as arising from thinned lithosphere, with greatest thinning to the southeast [Zorin *et al.*, 1989] beneath the Mongolian fold belt. Our earlier study [Gao *et al.*, 1994b] reported teleseismic travel time delays which correlate with the gravity, suggesting an asymmetric asthenospheric upwarp that peaks under Lake Baikal but is greater under the Mongolian fold belt than beneath the Siberian craton to the northwest. A subsequent study [Petit *et al.*, 1998] using regional events rather than teleseismic finds diametrically opposite results, with high velocities beneath the lake and fold belt, and low velocities in the mantle beneath the Siberian craton. Those authors suggest a narrow mantle plume reaches the bottom of the craton and follows its border in the Baikal area. A number of other workers argue for cold strong lithosphere beneath the rift based on the presence of a deep seismogenic zone [Deverchere *et al.*, 2001], or large values of the effective elastic thickness from flexure calculations using the gravity field [Diament and Kogan, 1990; Ruppel *et al.*, 1993; Petit *et al.*, 1997]. In particular, Petit *et al.* [1997] find an elastic thickness of approximately 30–50 km, and infer the mantle is strong to a depth of about 85 km. In this report we confirm the earlier result [Gao *et al.*, 1994b] that the lowest mantle velocities lie directly beneath the rift, and are at shallow depth. We find no evidence for low velocity associated with a plume under the Siberian craton. Given the low velocity, low gravity, low *Q* [Gao *et al.*, 1994b] and limited volcanism [Kiselev, 1987], our new results are compatible with sub-solidus, thermally modified mantle.

3. Data

[9] The teleseismic data set used in the study was collected by 28 short-period, three-component seismographs deployed along a 1280 km profile traversing the Siberian platform, Baikal rift zone, and the Mongolian fold

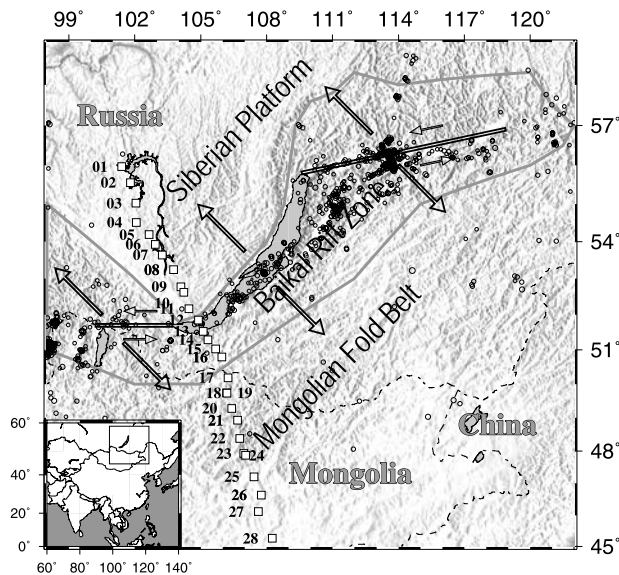


Figure 1. Topographic map of the Baikal rift zone and adjacent areas showing the locations of major tectonic units and seismic stations used in the study (squares). Arrows show regional stress fields of the Baikal rift zone obtained from surface geological structure analysis and earthquake focal mechanism studies [Sherman, 1992], and open circles are local events that occurred during the field experiment.

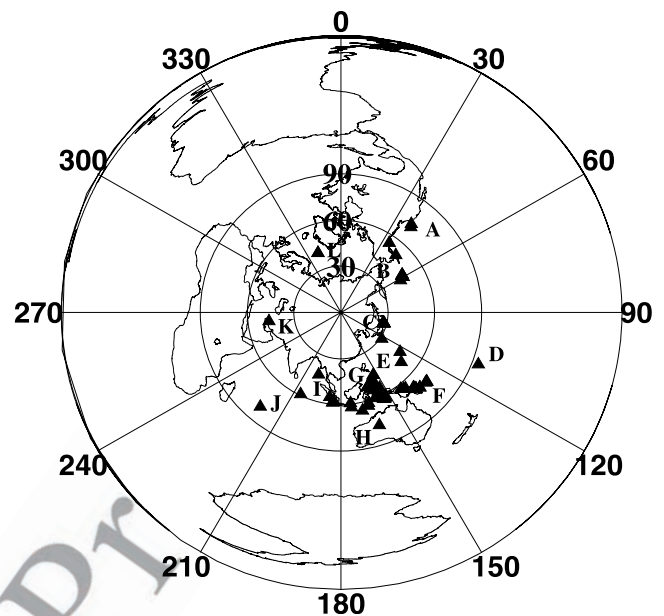


Figure 2. A map with azimuthal equidistant projection (which preserves distances and azimuths relative to the center of the projection) centered at station 13, showing epicenters of events (triangles) used in the study. Letters indicate names of event groups used for dividing and averaging the travel time residuals.

184 belt (Figure 1) in a 4-month period in 1992. All the
185 recorders were Refteks which digitized the seismic signals
186 continuously at 10 samples per second. The seismographs
187 frequently synchronized their internal clocks to timing
188 signals from the Omega navigation system (locked to
189 stations in Norway and Japan), which resulted in a timing
190 error for most of the seismograms of less than 20 ms.

191 [10] Our analysis is based on tomographic inversion of
192 teleseismic P wave travel time residuals. In order to obtain
193 those residuals, we first filter the seismograms in the 0.2–1.5
194 Hz frequency band, and manually pick the onset of the first
195 arrival. Only seismograms with a clear onset are used, and
196 those from an event are not used if the number of high-
197 quality travel time picks is less than 14 (out of a maximum of
198 28). A total of 1370 travel time picks from 77 events (Figure
199 2) in the epicentral distance from 28° to 93° are used to
200 invert for velocity structures beneath the profile. We then
201 correct the observed arrival times with theoretical arrival
202 times calculated using the IASP91 Earth model [Kennett and
203 Engdahl, 1991] and the EHB catalog [Engdahl et al., 1995].
204 Relative residuals are obtained by subtracting the event's
205 mean residual from the raw residuals.

206 [11] We further correct the relative residuals by removing
207 the slope on the residuals for each event, which is most
208 likely caused by mislocation of the events instead of
209 velocity gradients in the crust or upper mantle. The main
210 evidence for this conclusion is that while most of the events
211 located in nonsubduction zone areas such as the western
212 United States show near-zero slopes, events with slopes of
213 larger than 0.2 ms/km are all located in subduction zones,
214 where the near-source stations used to locate these events
215 are almost all on one side of the event, and hence a
216 systematic mislocation is plausible [Dziewonski and Ander-

217 son, 1981]. The error in the position and the origin time
218 must be compensated by an equivalent error in depth, which
219 can lead to a location-dependent tilt of a derived travel time
220 curve [Dziewonski and Anderson, 1981]. We calculated that
221 for an earthquake of intermediate focal depth, at 40° from
222 the center of the array, a 50-km depth mislocation causes a
223 slope error in the travel time residual curves of 0.3 ms/km
224 [Gao et al., 1994b]. Anisotropy in the subduction area can
225 also cause systematic mislocation of events when an iso-
226 tropic model is used for earthquake location [e.g., Kendall
227 and Thomson, 1993]. The final relative travel time residuals
228 after these corrections are shown in Figure 3.

229 [12] To study event location dependence of the relative
230 travel time residuals, we group the events by their back
231 azimuth (ϕ) and epicentral distance (Δ) relative to station

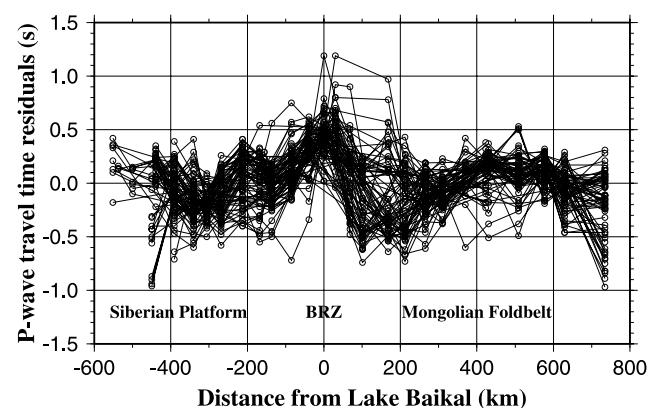


Figure 3. Corrected teleseismic P wave travel time residuals from 77 events plotted along the profile. The zero distance is station 13.

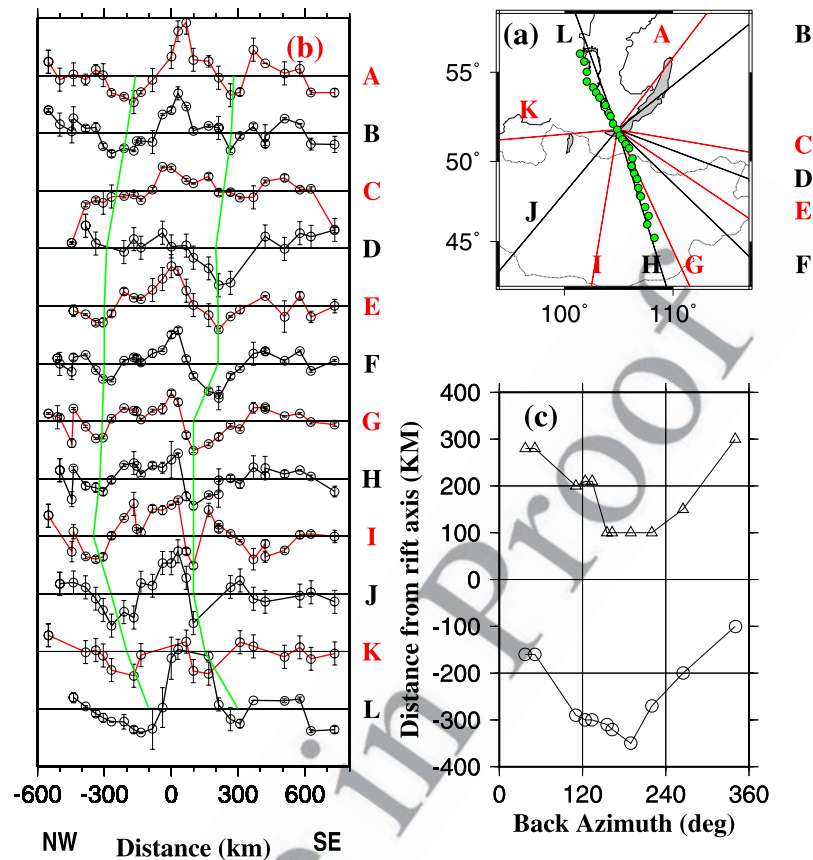


Figure 4. (a) A map showing the mean direction of arriving seismic rays from the 12 event groups (A–L). (b) Mean travel time residuals from the event groups. The two green lines represent locations of the flank lows on the travel time curves (except for group C, on which the flank lows are nonexistent). One grid on the vertical axis represents 1 s. (c) Location of the flank lows plotted against the mean back azimuth of each event group.

232 13, which is located near the south shore of Lake Baikal. 233 We divide the source regions on the Earth’s surface into 24 234 areas. Events within area (i, j) satisfy

$$(i - 1) * 30^\circ \leq \phi < i * 30^\circ, (i = 1, 2, \dots, 12), \quad (1)$$

236 and

$$(j - 1) * 60^\circ \leq \Delta < j * 60^\circ, (j = 1, 2). \quad (2)$$

239 [13] The 77 events used in the study occurred within 12 240 of the 24 areas (Figure 2). The number of events within each 241 group ranges from 1 to 20. To minimize the dominance of 242 the SE event groups in the final velocity model, we 243 calculate the average relative travel time residuals from 244 each group (Figure 4) and use those averaged residuals in 245 the inversions below (except for the block inversion which 246 uses the individual residuals). Most of the groups show a 247 positive residual (“central high”) of 0.2–1.0 s in the 248 distance range -50 to 50 km (Figure 4). In addition, all 249 but group C, which is the closest event group to the profile, 250 show an area of relatively early arrivals (“flank lows”) on 251 each side of the central high. The location of the lowest 252 point in the southern flank lows ranges from 100 km to 300 253 km from station 13, and that for the northern ones ranges 254 from -350 to -100 km (Figure 4c). A systematic pattern

can be observed when the locations are plotted against the 255 mean back azimuth of the event groups. Figure 4c indicates 256 that the flank lows shift northwestward for events from the 257 southeast, and southeastward for those from the northwest. 258 In spite of the systematic variation of the locations with 259 back azimuth, the distance between the two flank lows 260 remains approximately constant regardless of the back 261 azimuth (Figure 4). 262

4. Inversion of Travel Time Residuals 263

[14] We used three techniques to invert the travel time 264 residuals to obtain P wave velocity structures beneath the 265 profile. The first technique assumes that the residuals are 266 mostly caused by the lithosphere/asthenosphere interface 267 and solves for the spatial variation of that interface. The 268 second technique is the standard ACH block inversion 269 scheme [Aki *et al.*, 1977], and the third technique is basically 270 a modification of the first one by introducing transverse 271 isotropy with a vertical symmetry axis in the asthenosphere. 272

4.1. Lithosphere/Asthenosphere Interface: 273 Isotropic Model 274

[15] Under the assumption that the travel time residuals 275 are primarily caused by the spatial variation of the depth of 276 the lithosphere/asthenosphere interface, we construct an 277

278 initial model based on the first-order features of the travel
 279 time residuals. The existence and the appearance of the
 280 peaks in the distance range of -50 to 50 km imply an
 281 upwarped low-velocity structure in the vicinity of the rift
 282 axis. The two flank lows on travel time residual curves on
 283 each side of the rift, the approximately constant distance
 284 between them, and the large and systematic location shift
 285 for events from different azimuths (Figure 4) can be caused
 286 by two high-velocity structures (among other possibilities as
 287 discussed below). To estimate the scale of such structures,
 288 we search for the optimal depth (d) and location (x_0) of a
 289 rift-parallel high-velocity cylinder on each side of the rift by
 290 fitting the observed azimuthal dependence of the locations
 291 (Figure 4c) using $x = x_0 - d \cdot \tan(\theta) \cdot \cos(\phi)$, where x is the
 292 observed location of the travel time lows associated with the
 293 cylinders, x_0 is the horizontal location relative to station 13,
 294 d is the depth of the cylinder, θ is the angle of incidence,
 295 ϕ and is the back azimuth relative to the SE strike of the
 296 profile. The best fitting parameters are $x_0 = -220$ km and
 297 $d = 235$ km for the northern cylinder, and $x_0 = +205$ km
 298 and $d = 160$ km for the southern cylinder. The calculated
 299 locations using those parameters are well matched by the
 300 observed ones (Figure 5).

301 [16] Studies in the BRZ [e.g., Logatchev and Zorin, 1992;
 302 Gao et al., 1994b] and in other rift zones [e.g., Parker et al.,
 303 1984; Dahlheim et al., 1989; Davis, 1991; Davis et al.,
 304 1984, 1993; Slack et al., 1994, 1996] reveal that the velocity
 305 contrast between the upwarped asthenosphere and the
 306 velocity of the surrounding areas is about 3–12%. In
 307 addition, the location of the highest point of the upwarped
 308 asthenosphere, which might have reached the Moho, may or
 309 may not be directly beneath the rift axis.

310 [17] Given the above a priori information, we represent the
 311 geometry of the lithosphere/asthenosphere interface using
 312 the combination of a cosine and a Gaussian function, i.e.,

$$f(x) = -h_0 + f_1(x) * f_2(x), \quad (3)$$

314 where

$$f_1(x) = \begin{cases} a_1 * \cos(2\pi x/\lambda) & |x| \leq 3\lambda/4 \\ 0 & \text{elsewhere} \end{cases} \quad (4)$$

316 and

$$f_2(x) = \exp(-0.5x^2/\sigma^2), \quad (5)$$

318 where h_0 is the depth of the lithosphere outside the
 319 anomalous region, a_1 is the magnitude of the upwarp, λ is
 320 the wavelength of the cosine function, σ and is the standard
 321 deviation of the Gaussian function.

322 [18] Numerical tests show that $f(x)$ is a function with great
 323 flexibility. Some of the features of $f(x)$ include (1) the flank
 324 lows occur at $|x| \leq \lambda/2$; (2) when $\lambda/\sigma > 6$ the magnitude of
 325 the two flank lows reduces to nearly zero; and (3) the
 326 magnitude of the central high \geq that of the flank lows.

327 [19] To allow for the possible asymmetric shape of the
 328 upwarp, we give each side an independent λ and σ . The
 329 strike and location of the vertex line of the two-dimensional
 330 structure are also treated as unknown parameters.

331 [20] In summary, there are nine unknown parameters to
 332 be found through nonlinear inversion. They are (1) a_1 ,

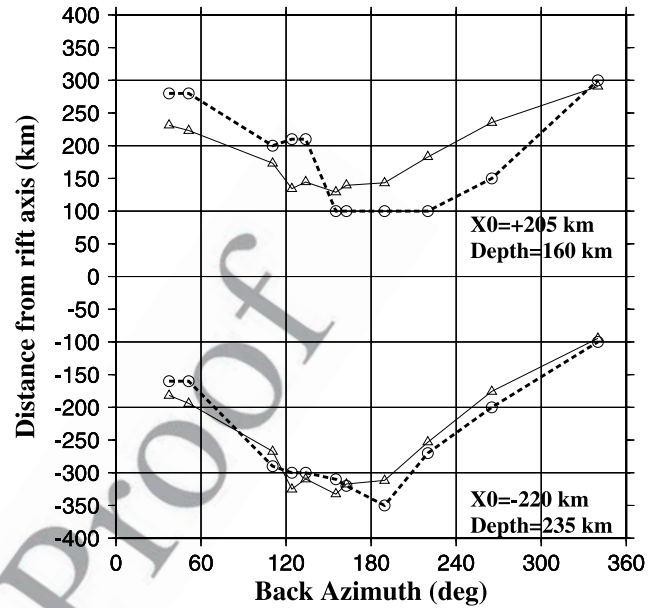


Figure 5. Observed (circles) and fitted (triangles) locations of the two flank lows. X_0 and depth are the optimal locations and depths of the imaginary rift-parallel high-velocity cylinders.

333 magnitude of the upwarp; (2) λ_1 , wavelength of the left
 334 cosine function; (3) σ_1 , standard deviation of the left
 335 Gaussian function; (4) λ_2 , wavelength of the right cosine
 336 function; (5) σ_2 , standard deviation of the right Gaussian
 337 function; (6) γ , asthenospheric-lithospheric velocity con-
 338 trast; (7) ϕ_0 , strike of the structure measured anticlockwise
 339 from the east; (8) b , location of the vertex line of the 2-D
 340 structure; and (9) h_0 , depth of normal lithosphere.

341 [21] We use a three-dimensional downward projection
 342 method [Davis et al., 1984; Gao et al., 1994b] and a
 343 nonlinear Bayesian inversion technique [Jackson and Mat-
 344 su'ura, 1985; Jackson, 1972] to estimate the parameters.
 345 The method assumes straight rays and a plane wave approx-
 346 imation. The resulting parameters are (1) $a_1 = 153 \pm 10$ km;
 347 (2) $\lambda_1 = 518 \pm 15$ km; (3) $\sigma_1 = 171 \pm 10$ km; (4) $\lambda_2 = 505 \pm$
 348 25 km; (5) $\sigma_2 = 132 \pm 10$ km; (6) $\gamma = (2.4 \pm 0.05)\%$; (7) $\phi_0 =$
 349 $31.6 \pm 0.7^\circ$; (8) $b = 14 \pm 25$ km; and (9) $h_0 = 198 \pm 25$ km.
 350 The resulting lithosphere/asthenosphere interface is shown
 351 in Figure 6.

352 [22] Some main features of the interface include the
 353 following: (1) the asthenosphere reaches to $h_0 - a_1 = 45$
 354 ± 15 km depth; (2) the magnitude of the flank lows is about
 355 60 km for the left one, and 40 km for the right one; (3) the
 356 velocity contrast between the lithosphere and the astheno-
 357 sphere is 2.4%; (4) the strike of the structure is 31.6°
 358 measured anticlockwise from the east, which is smaller
 359 than the general direction of the strike of the BRZ (55°),
 360 but it is close to the local strike of the rift; and (5) the vertex
 361 line of the 2-D structure is about 14 km south of station 13,
 362 i.e., close to the rift axis.

4.2. Block Inversion

363 [23] We next invert the travel time residuals using the 3-D
 364 ACH block inversion method [Aki et al., 1977]. The layer
 365 thicknesses are chosen so that the time a ray spends in each
 366

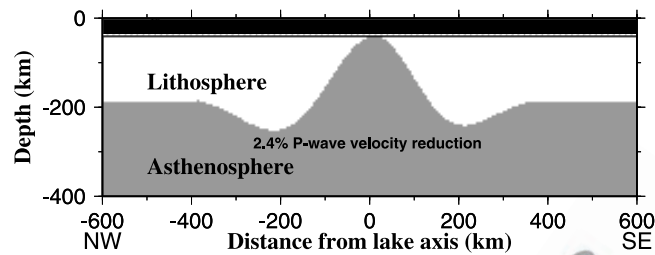


Figure 6. Results of travel time inversion under the assumption that travel time variations are mostly caused by spatial variation of the depth of the lithosphere/asthenosphere interface.

367 layer is approximately the same for all layers. Because the
 368 mean station spacing is about 50 km, the horizontal dimen-
 369 sions of the blocks are chosen as 80 km. To determine the
 370 optimum depth for the tomography model, we ran a series of
 371 inversion with models of different depth. We then plotted the
 372 misfits, which are defined as $\xi = \sum_{i=1}^N (t_i - t_i^{fit})^2 / (N - M)$,
 373 where N is the number of data points, M is the number of
 374 parameters, and t_i and t_i^{fit} are the observed and fitted travel
 375 time residuals, against the depths, and we found that the
 376 misfits stopped decreasing significantly when depth ≥ 400
 377 km. Thus we choose 410 km, which is the mean global
 378 depth of the bottom of the upper mantle, as the bottom of
 379 the area with lateral velocity variations. The optimum
 380 damping parameter, which controls the smoothness of the
 381 resulting velocity model, was determined by running a
 382 series of models with damping parameters from 10 to
 383 200. Obviously, a larger damping parameter corresponds to
 384 a larger misfit. We chose the optimum damping param-
 385 eter as the one at which the slopes of the misfits versus
 386 damping parameters curve changes significantly. It turns out
 387 that the value is about 56.

388 [24] The resulting velocity slices are shown in Figures 7
 389 and 8. A low-velocity body is observed in the vicinity of the
 390 rift axis in the top 300 km of the Earth, and a high-velocity
 391 body is observed on each side of the rift in the top 210 km.
 392 In the 125–210 km depth range, the width of the low-
 393 velocity body is about 200 km. The centers of the high-
 394 velocity bodies are located at about 200 km from the rift
 395 axis. The maximum velocity contrast is about 3%. These
 396 results are consistent with those obtained under the assump-
 397 tion that most of the travel time residuals are caused by the
 398 spatial variation in the depth of the lithosphere/astheno-
 399 sphere interface (Figure 6).

400 [25] Also shown on Figures 7 and 8 are the resolution and
 401 uncertainties from the inversion, which indicate the regions
 402 of the model that are well resolved and modeled by the data.
 403 For each layer the blocks within the solid lines have
 404 resolution values of 0.7 or greater. Hence these regions of
 405 the model are well resolved by the data. The blocks within
 406 the dotted lines have standard errors of 0.6% or less. For the
 407 upper two layers of the model, 40 to 125 km and 125 to 210
 408 km deep, the velocity contrasts modeled by the data vary
 409 from $-2 \pm 0.6\%$ to $+1 \pm 0.6\%$ in the well resolved region of
 410 the model. This two to three percent velocity contrast is
 411 significantly greater than the uncertainty. For the lower two
 412 layers, deeper than 210 km, the magnitude of the velocity
 413 contrast is significantly smaller. The lower layers have
 414 velocity contrasts on the order of 1%. Given the 0.6%
 415 uncertainty for these blocks, the inversion results are con-

sistent with a smooth asthenosphere or limited velocity
 variations in the asthenosphere beneath the rift.

4.3. Lithosphere/Asthenosphere Interface: Transversely Isotropic Model

[26] In this section, we use a transversely isotropic
 asthenosphere with vertical axis of symmetry to interpret
 the travel time residuals. The use of an anisotropic model is
 mainly motivated by the two flank lows observed on the
 travel time residual curves (Figure 4) and by the fact that
 other studies such as deep seismic sounding and gravity,
 among others, do not support the existence of a high-
 velocity body in the areas beneath where the flank lows
 are observed (see section 5.1). Furthermore, there is grow-
 ing evidence that both the lithosphere and asthenosphere are
 anisotropic with a fabric that is controlled by shear defor-
 mation associated with the movement of mantle flow
 [Kendall, 1994; Blackman *et al.*, 1996; Montagner and
 Guillot, 2000]. The shears associated with mantle flow in
 a localized convection cell [e.g., Huismans *et al.*, 2001,
 Plate 1] from the upward and downward flanking flows will
 give a complex distribution of anisotropy that is beyond the
 ability of teleseismic residuals to resolve. We thus consider
 a gross simplification of the true situation. Near vertically
 incident P waves will be most influenced by fabrics caused
 by vertical shears. We use a model consisting of a low-
 velocity asthenospheric upwarp and an underlying flat
 asthenospheric layer of laterally variable anisotropy. We
 assume that the lithosphere is isotropic for steeply incident
 teleseismic P waves, and both the upwarped and flat parts of
 the asthenosphere are transversely isotropic with a vertical
 axis of symmetry. As discussed below, the observed travel
 time residuals require an anisotropy of about 3% in the
 mantle to the depth of about 400 km. While most studies
 suggest that anisotropy is mostly limited in the top 250 km
 of the Earth, some other studies find radial anisotropy at
 about 400 km depth beneath large areas such as the western
 Pacific Ocean [Boschi and Dziewonski, 2000], and azimu-
 thal anisotropy in the mantle transition zone [Trampert and
 van Heijst, 2002].

[27] A P wave with vertical incidence traveling through a
 transversely isotropic medium with vertical axis of symme-
 try has the highest velocity, and that with horizontal
 incidence has the lowest velocity. For nonvertical incidence,
 the velocity, $V_p(\theta)$, can be calculated using the result of
 Backus [1965] and its modified forms. One of the most
 frequently used forms for transversely isotropic media is

$$V_p^2(\theta) - V_0^2 = c_1 \cos(2\theta) + c_2 \cos(4\theta), \quad (6)$$

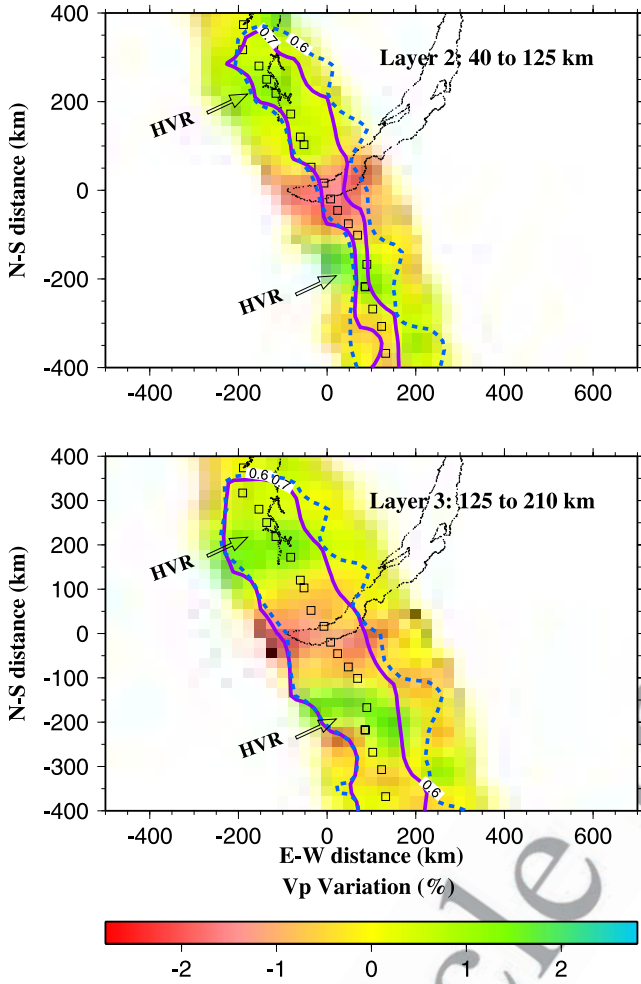


Figure 7. Smoothed ACH block inversion of travel time residuals for the two upper mantle layers in the lithosphere. Open squares are the stations. The solid line indicates the contour of blocks with 0.7 resolution; blocks within the contour are resolved at 0.7 or greater. The dotted line indicates the contour of blocks with standard errors of 0.6%; blocks within the contour have errors of 0.6% or less. The region within the contours are well resolved and modeled by the data. HVR, high-velocity region.

463 where V_0 is the mean velocity, θ is the angle between the
 464 symmetry axis and the ray direction, c_1 and c_2 are
 465 combinations of four elastic constants, $c_1 = (c_{11} - c_{22})/2$;
 466 $c_2 = (c_{11} + c_{22})/8 - c_{12}/4 - c_{66}/2$ [Bamford, 1977; Crampin
 467 and Bamford, 1977; Fuchs, 1984; Anderson, 1989].

468 [28] We assume that the magnitude of anisotropy is the
 469 highest beneath the rift axis and decreases exponentially
 470 outward; that is, c_1 and c_2 above are considered to be
 471 Gaussian functions of distance from the rift axis with the
 472 forms

$$c_1(x) = c_{10} \exp(-0.5x^2/\sigma^2) \quad (7)$$

474 and

$$c_2(x) = c_{20} \exp(-0.5x^2/\sigma^2), \quad (8)$$

where σ is the standard deviation of the Gaussian function. 476
 To include possible asymmetric decay of the magnitude of 477
 anisotropy, a different σ is used for $x < 0$ and $x > 0$. 478

[29] Figure 9 (top) shows travel time residuals in three 479
 scenarios for a ray with $\theta = 10^\circ$. When the flat astheno- 480
 spheric layer is isotropic, the residual curve consists of 481
 positive values with the peak near the center; when the 482
 upwarded asthenosphere is absent, the residuals are all 483
 negative with the minimum value near the center due to 484
 lateral variation of anisotropy in the underlying astheno- 485
 sphere. When both parts of the asthenosphere are present 486
 and are anisotropic, the combined travel time residual 487
 curve has a valley on each side of the rift and a reduced 488
 peak near the center. 489

[30] Because of the largely 1-D configuration of our array 490
 (Figure 1), we assume that the structure is two-dimensional 491
 beneath the array. The surface of the upwarp is described 492
 using a parabola of the form 493

$$z(x) = a_1 + \lambda x^2, \quad (9)$$

where a_1 is the depth of the peak of the upwarp and λ is 495
 the coefficient of the parabola. To include a possible 496
 asymmetric shape of the upwarp, an independent λ is used 497
 for $x < 0$ and $x > 0$. The strike and location of the vertex 498

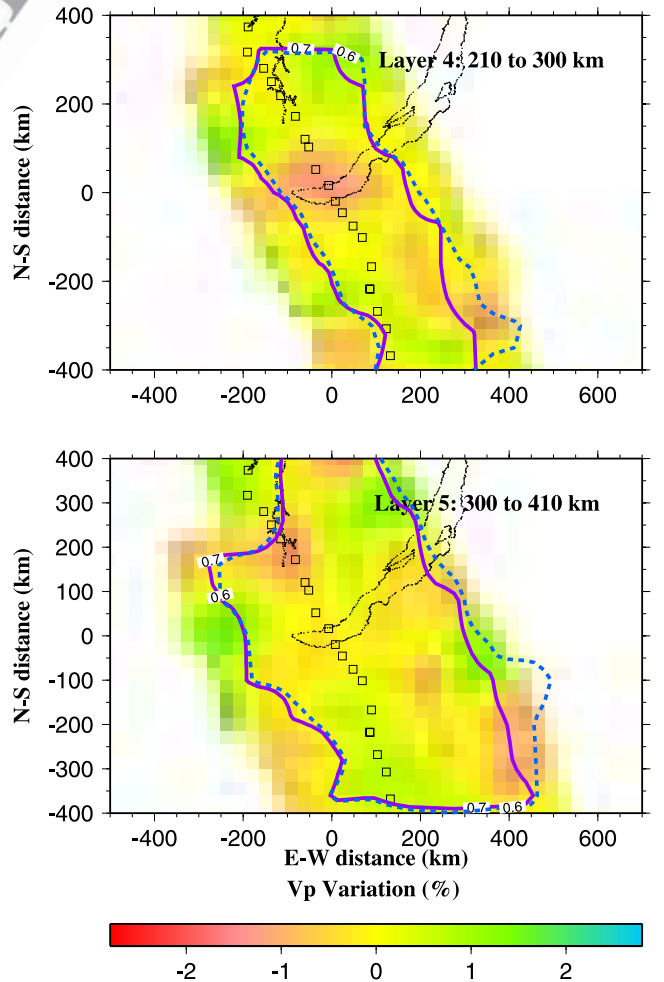


Figure 8. Same as Figure 7 but for the two upper mantle layers below the lithosphere.

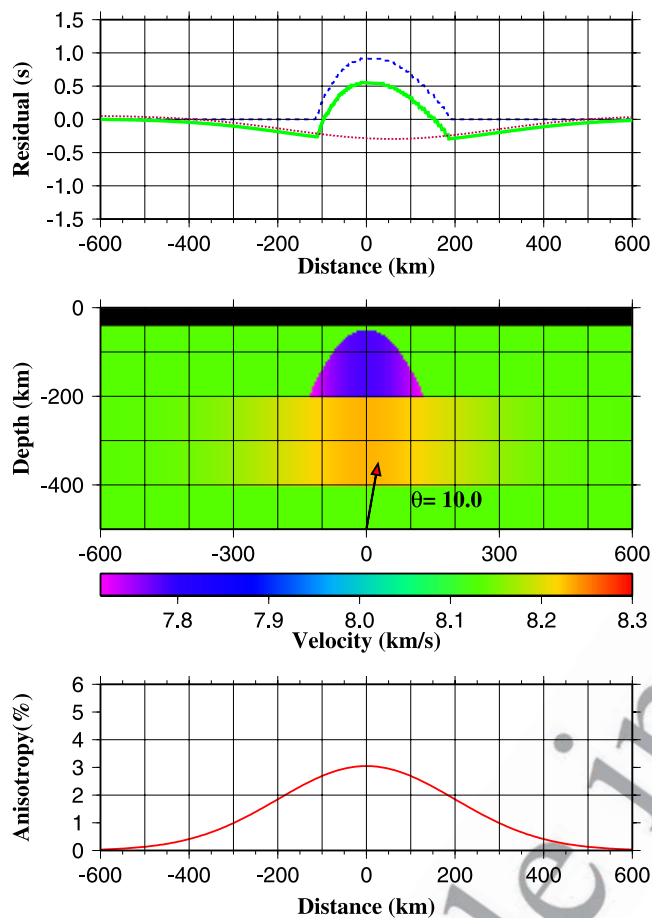


Figure 9. (middle) Velocity model, (top) theoretical travel time residuals computed for a P wave with 10° incident angle, and (bottom) vertical anisotropy across the profile. The model is composed of an anisotropic low-velocity upwarp and a flat layer of anisotropic asthenosphere. The anisotropic media are transversely isotropic with vertical axis of symmetry. The travel time residuals are computed for the cases: (1) when the flat asthenospheric layer of anisotropy is absent (dashed blue line); (2) when the upwarp is absent (dotted red line); and (3) when both are present (solid green line).

528 of the two-dimensional structure will also be treated as
529 unknown parameters.

530 [31] In summary, there are in total twelve unknown
531 parameters to be found by the inversion. They are (1) a_1 ,
532 depth of the upwarp; (2) λ_1 , coefficient of the left (north-
533 west) parabola; (3) λ_2 , coefficient of the right (southeast)
534 parabola; (4) γ , asthenospheric/lithospheric velocity con-
535 trast; (5) c_{10} , magnitude of anisotropy parameter 1; (6) c_{20} ,
536 magnitude of anisotropy parameter 2; (7) σ_1 , standard
537 deviation of the left Gaussian function; (8) σ_2 , standard
538 deviation of the right Gaussian function; (9) ϕ_0 , strike of the
539 structure measured anticlockwise from the east; (10) b ,
540 location of the vertex line of the 2-D structure; (11) h_1 ,
541 thickness of the flat asthenospheric anisotropy layer; and
542 (12) h_0 , depth of the base of the upwarp.

543 [32] We employ the 3-D downward projection method
544 used in section 4.1 (with slight modifications to account for
545 the anisotropy) to estimate the parameters. The resulting

parameters from Bayesian inversion are (1) $a_1 = 45 \pm 15$ 546
km; (2) $\lambda_1 = 0.00877 \pm 0.00065 \text{ km}^{-1}$; (3) $\lambda_2 = 0.01363 \pm$ 547
 0.00070 km^{-1} ; (4) $\gamma = 2.53 \pm 0.09\%$; (5) $c_1 = 1.573 \pm 0.053$ 548
 km^2/s^2 ; (6) $c_2 = -0.692 \pm 0.052 \text{ km}^2/\text{s}^2$; (7) $\sigma_1 = 350 \pm 125$ 549
km; (8) $\sigma_2 = 170 \pm 40 \text{ km}$; (9) $\phi_0 = 51.8^\circ \pm 0.8^\circ$; (10) $b = 33$ 550
 $\pm 20 \text{ km}$; (11) $h_1 = 170 \pm 20 \text{ km}$; and (12) $h_0 = 230 \pm 30 \text{ km}$. 551

[33] The resulting velocity model is shown in Figure 10, 552
in which a localized velocity model [Egorkin *et al.*, 1984] 553
was used as the reference model. The results indicate that 554
the low-velocity upwarp starts at a depth of 230 km and 555
reaches 45 km depth. The velocity inside the upwarp is 556
2.5% lower than the outside velocity at the same depth. At 557
its bottom the upwarp is about 260 km wide. The strike of 558
the structure is 52° measured anticlockwise from the east, 559
and the vertex of the 2-D structure is 33 km south of station 560
13. The inversion indicates that the vertex of the 2-D 561
structure is approximately parallel to the axis of the surficial 562
manifestation of the rift. 563

5. Discussion 565

5.1. Applicability of the Velocity Models 566

[34] Three techniques were used to invert the same P wave 567
travel time residual data set for upper mantle velocities. 568
Results from the two techniques under the assumption of 569
isotropy (Figures 6–8) are consistent with each other. The 570
major difference between the isotropy and anisotropy results 571
is that in the isotropic models, the flank lows in the travel time 572
curves (Figure 4) are caused by high-velocity bodies that are 573
parallel to the rift axis, and in the anisotropic model, they are 574
related to anisotropy with a vertical axis of symmetry. 575

[35] The final misfits are 0.046, 0.017, and 0.057 s^2 for 576
the models presented in sections 4.1, 4.2, and 4.3, respec- 577
tively. The small misfit (0.017) for the block inversion 578
technique is probably the result of using a more realistic a 579
3-D model rather than a 2-D one. To test this hypothesis, we 580
ran an ACH inversion using a 2-D model for the same data 581
set, and found that the misfit is 0.037 s^2 , which is com- 582
parable with those from the other two techniques. Thus it is 583
impossible to distinguish between these models based on 584
the goodness of fit of the P wave travel time residuals alone. 585
In addition, it is clear that a model with the best fit to data 586
may not necessarily be the most reasonable one physically. 587
Therefore other types of geophysical measurements that are 588
independent from teleseismic P wave travel time residuals 589
are needed to determine the applicability of the models. 590

5.1.1. Results From Deep Seismic Sounding 591

[36] Deep seismic sounding experiments started in the 592
former USSR in 1968. A total length of profiles of more 593
than 4000 km covering an area of over 400,000 km^2 have 594
been studied, and one profile extended across the southern 595
Baikal area [Puzyrev *et al.*, 1978]. The investigation dis- 596
covered a low-velocity upper mantle layer in the area but 597
did not find any indication of lithospheric downwarp. This 598
technique uses near-horizontal refracted rays, which may be 599
less sensitive to the vertical fabrics than teleseismic P 600
waves. 601

5.1.2. Bouguer Gravity Anomalies 602

[37] On the basis of Birch's law, a 3% increase in seismic 603
velocity at the base of the lithosphere leads to an increase of 604
about 110 kg/m^3 in density. Given the geometry and depth 605
of the two high-velocity downwarps (Figure 6), we calcu- 606

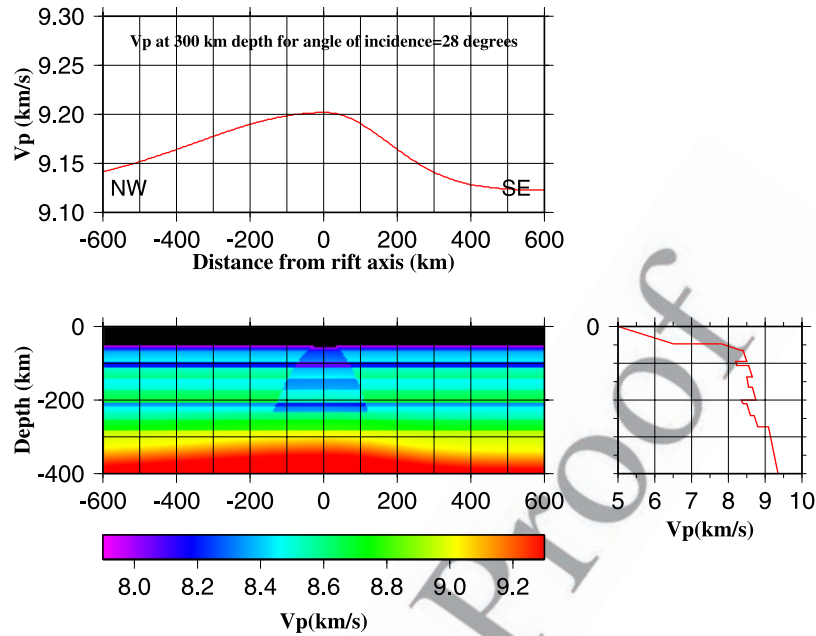


Figure 10. (bottom left) P wave velocity model derived from inversion of travel time residuals under the assumption of transverse isotropy. Both the flat and the upwarped parts of the asthenosphere are anisotropic, although the anisotropy in the latter cannot be visually observed. (top) P wave velocity at 300 km depth for rays with an angle of incidence of 28° . The velocity variations are the effect of anisotropy with a vertical axis of symmetry. (bottom right) Plot of isotropic V_p as a function of depth in the regions outside the upwarped area [Egorkin *et al.*, 1984].

607 lated that a broad positive gravity anomaly with a maximum
608 value of about 30 mGal would have been observed if the
609 downwarps have a correlated density anomaly. As shown in
610 Figure 11, such anomalies are not observed from existing
611 gravity data in the study area [e.g., Zorin *et al.*, 1989;
612 Kaban *et al.*, 1999]. In particular on the Siberian craton, the
613 gravity is flat, whereas to the south large negative values are
614 observed probably in part due to thickened crust in the
615 Mongolian fold belt. Therefore the isotropic models are not
616 supported by available gravity data.

5.1.3. Surface Topography

617 [38] To maintain isostatic balance, a broad high-density
618 downwarp of the base of the lithosphere should be com-
619 pensated by a broad depression of the surface of the Earth.
620 Using the densities given in the IASP91 Earth model, we
621 estimated that the magnitude of the depression would be as
622 large as 1.4 km in order to reach compensation. Analysis of
623 digital elevation data across the profile reveals that such
624 depressions do not exist at the expected locations.

5.1.4. Crustal Thickness

626 [39] In the absence of a surface depression, a thickened
627 crust in the area above the lithospheric downwarps could
628 also compensate the excessive mass created by the litho-
629 spheric downwarps because the crust has a lower density
630 than the lithosphere. We calculated that a thickening directly
631 above the downwarps of about 10 km is needed, which is
632 not observed by stacking P -to- S converted phases from the
633 Moho [Zachary *et al.*, 2000].

5.2. A Small-Scale Mantle Convection System Beneath the BRZ

635 [40] Independent geophysical measurements described in
636 the above section suggest that an anisotropic model is a
637
638

639 more plausible explanation for the travel times than the
640 isotropic ones. Convective shear should cause lattice-pre-
641 ferred orientation (LPO) of crystallographic axes of aniso-
642 tropic upper mantle minerals such as olivine, which is
643 thought to comprise about 60% of the Earth's uppermost

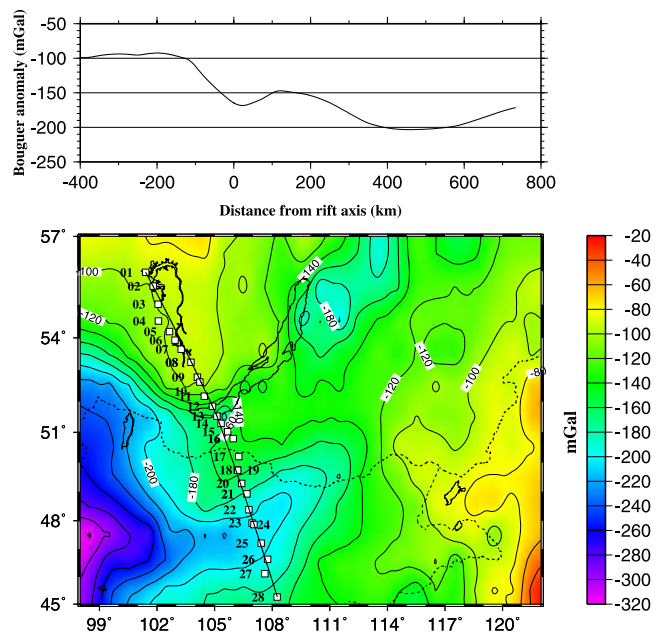


Figure 11. (bottom) Regional Bouguer gravity anomalies (averaged in 1° by 1° blocks) in the study area (data after Kaban *et al.* [1999]), and (top) gravity profile along the seismic line.

644 mantle. The a axis of olivine aligns in the flow direction
 645 under progressive simple shear [e.g., Hess, 1964; Karato,
 646 1989; Babuska and Cara, 1991; Silver and Chan, 1991;
 647 Chastel et al., 1993; Silver, 1996]. For example, in a
 648 medium that is composed of pure olivine with perfectly
 649 aligned a axis and randomly aligned b and c axes in the
 650 plane perpendicular to a , seismic P waves traveling along
 651 the a axis have a velocity that is about 20% faster than P
 652 waves traveling orthogonal to it.

653 [41] We propose that vertical asthenospheric flow is
 654 responsible for generating the observed transverse isotropy
 655 beneath the BRZ and that the flow could be the ascending
 656 and descending branches of a small-scale convection system
 657 associated with the rifting [Huismans et al., 2001]. The
 658 presence of SKS splitting in the BRZ area [Gao et al.,
 659 1994a, 1997] implies anisotropy with horizontal symmetry
 660 axes are present. Because olivine is near-hexagonal with a
 661 axis being dominantly fast, we have used a transversely
 662 isotropic model and assumed that the P waves are sensitive
 663 to the vertical distribution of a axes, and the splitting to the
 664 horizontal distribution of a axes. In contrast to vertically
 665 traveling P waves, SKS splitting is more sensitive to the
 666 horizontal shears and therefore to the horizontal branches of
 667 the convection. Shear wave splitting measurements in the
 668 Baikal region [Gao et al., 1994a, 1997] reveal systematic
 669 spatial variations in the fast shear wave polarization direc-
 670 tions. In the inner region of the BRZ, the fast directions are
 671 distributed in two orthogonal directions, NE and NW,
 672 approximately parallel and perpendicular to the NE strike
 673 of the rift. In the adjacent Siberian platform and northern
 674 Mongolian fold belt, only the rift-orthogonal fast direction
 675 is observed. The rift-parallel fast directions near the rift axes
 676 can be interpreted by oriented magmatic cracks in the
 677 mantle or small-scale mantle convection with rift-parallel
 678 flow [e.g., as described by Nicholas, 1993], and rift-ortho-
 679 gonal fast directions could be interpreted as the result of the
 680 horizontal component of a small-scale mantle convection
 681 system centered at the rift axis. Our results from the travel
 682 time residual inversion under the assumption of transverse
 683 isotropy (Figure 10) provide further supportive evidence for
 684 the existence of such a convection system.

685 5.3. Speculation on the Existence of Flank Lows in 686 Other Rifts

687 [42] During the past 20 years several teleseismic experi-
 688 ments were conducted across the Rio Grande and East
 689 African rifts [Davis, 1991; Davis et al., 1993; Achauer et
 690 al., 1994; Slack et al., 1994, 1996; Ritsema et al., 1998].
 691 While the area covered by late travel times is wider across
 692 both rifts than that across the BRZ (which implies that the
 693 asthenospheric upwarps are wider than that beneath BRZ)
 694 and the peak-to-peak anomalies are about twice as large, the
 695 rift-orthogonal dimensions of the seismic arrays deployed
 696 in those experiments were not as large as that of the BRZ.
 697 Therefore it is possible that similar flank lows, if they exist
 698 beneath those rifts, could be located outside the arrays. It is
 699 interesting to note that there is indeed an area with early
 700 arrivals of as large as 1 s located about 230 km east of the
 701 axis of the Rio Grande rift, and 270 km west of the eastern
 702 end of the E-W seismic profile [Davis, 1991, Figure 3].
 703 This flank low is observed on events from the SE direction,
 704 but is not seen on events from the NW direction. This could

suggest that the flank low shifts southeastward for events
 from the NW and consequently develops beyond the limits
 of the array. It seems that a teleseismic profile of about
 1500 km long is needed across both the Rio Grande and
 East African rifts in order to study the existence and
 characterization of possible flank lows associated with
 those rifts.

6. Conclusions

[43] Nonlinear inversion of travel times and other geo-
 physical measurements suggest that the travel time residuals
 observed along a 1280 km profile across the Baikal rift zone
 are the combined results of an upwarped asthenosphere and
 a vertical mantle flow centered at the rift axis. An isotropic
 inversion gives rise to asthenospheric upwarp beneath the
 rift and lithospheric downwarps on either side. However the
 downwarps are not seen in the gravity, or, if isostatically
 compensated, in the topography or crustal thickness. Further
 they have not been recorded in previous deep seismic
 sounding experiments carried out in the area. One way to
 have large velocity anomalies without gravity effects is the
 presence of anisotropy. Previous SKS splitting had shown
 laterally variable splitting in the Baikal rift zone and was
 interpreted as caused by small scale convection. The P wave
 residuals and gravity can be explained if the vertical shears
 associates with mantle upwelling and downwelling cause a
 axes of olivine to be oriented vertically, and consequently
 cause a localized high-velocity anomaly beneath the rift
 zone. This superimposed on the low-velocity anomaly of
 asthenospheric upwarp gives rise to the characteristic cen-
 tral high and flanking lows in the travel time patterns. The
 results lend weight to models of active rifting induced by
 instability of the mantle lithosphere that causes small-scale
 convection to develop, in which lithospheric extension is
 much greater than crustal extension.

[44] This study demonstrates the role that anisotropy can
 play in the inversion of seismic travel time residuals, and the
 significance of shear wave splitting and travel time model-
 ing in detecting mantle convection systems. It also suggests
 the need for future seismic experiments along arrays that are
 significantly longer than most of the previous arrays across
 major continental rifts.

[45] **Acknowledgments.** This study has benefited from discussion
 and cooperation with the late Bob Meyer and his group at the University
 of Wisconsin, Madison. The data set used in the study were collected in a
 collaborative field program involving a team of seismologists from the
 Institute of Earth's Crust, Irkutsk, Siberia, Institute of the Physics of the
 Earth, University of Wisconsin, and University of California, Los Angeles.
 The gravity data set used for calculating Bouguer anomalies (Figure 11)
 was kindly provided by Peter Schwintzer. The paper benefited greatly from
 reviews provided by Andrew Nyblade and an anonymous reviewer. This
 study was supported by DARPA under contracts F2901-91-K-DB17 and
 F49620-94-1-0161, and by NSF under contract EAR-01-07055.

References

- Achauer, U., A. Glahn, J. P. R. Ritter, P. K. H. Maguire, P. Davis, P. Slack,
 and V. Green, New ideas on the Kenya rift based on the inversion of the
 combined data set of the 1985 and 1989/1990 seismic tomography ex-
 periments, *Tectonophysics*, 236, 305–329, 1994.
 Aki, K., A. Christofferson, and E. S. Husebye, Determination of the three-
 dimensional seismic structure of the lithosphere, *J. Geophys. Res.*, 82,
 277–296, 1977.
 Anderson, D. L., *Theory of the Earth*, 366 pp., Blackwell Sci., Malden,
 Mass., 1989.

705
706
707
708
709
710
711
713
714
715
716
717
718
719
720
721
722
723
724
725
726
727
728
729
730
731
732
733
734
735
736
737
738
739
740
741
742
743
744
745
746
747
748
749
750
751
752
753
754
755
756
757
758
759
760
761
762
763
764
765
766
767

- Anderson, D. L., The sublithospheric mantle as the source of continental flood basalts: The case against the continental lithosphere and plume head reservoirs, *Earth Planet. Sci. Lett.*, 123(1-4), 269-280, 1994.
- Babuska, V., and M. Cara, *Seismic Anisotropy in the Earth*, 217 pp., Kluwer Acad., Norwell, Mass., 1991.
- Backus, G. E., Possible forms of seismic anisotropy of the upper-most mantle under oceans, *J. Geophys. Res.*, 70, 3429-3439, 1965.
- Bamford, D., *Pn* velocity anisotropy in a continental upper mantle, *Geophys. J. R. Astron. Soc.*, 49, 29-48, 1977.
- Bjarnason, I. T., C. J. Wolfe, S. C. Solomon, and G. Gudmundson, Initial results from the ICEMELT experiment—Body-wave delay times and shear-wave splitting across Iceland, *Geophys. Res. Lett.*, 23, 459-462, 1996.
- Blackman, D. K., J.-M. Kendall, P. R. Dawson, H.-R. Wenk, D. Boyce, and J. P. Morgan, Teleseismic imaging of subaxial flow at mid-ocean ridges: Travel-time effects of anisotropic mineral texture in the mantle, *Geophys. J. Int.*, 127, 415-426, 1996.
- Boschi, L., and A. M. Dziewonski, Whole earth tomography from delay times of *P*, *PcP*, and *PKP* phases: Lateral heterogeneities in the outer core or radial anisotropy in the mantle?, *J. Geophys. Res.*, 105, 13,675-13,696, 2000.
- Chastel, Y. B., P. R. Dawson, H. R. Wenk, and K. Bennett, Anisotropic convection with implications for the upper mantle, *J. Geophys. Res.*, 98, 17,757-17,771, 1993.
- Crampin, S., and D. Bamford, Inversion of *P*-wave velocity anisotropy, *Geophys. J. R. Astron. Soc.*, 49, 123-132, 1977.
- Dahlheim, H.-A., P. M. Davis, and U. Achauer, Teleseismic investigation of the East African Rift-Kenya, *J. Afr. Earth Sci.*, 8(2-4), 461-470, 1989.
- Davis, P. M., Continental rift structures with reference to teleseismic studies of the Rio Grande and East African rifts, *Tectonophysics*, 197, 309-325, 1991.
- Davis, P. M., E. C. Parker, J. R. Evans, H. M. Iyer, and K. H. Olsen, Teleseismic deep sounding of the velocity structure beneath the Rio Grande Rift, *Field Conf. Guideb. N. M. Geol. Soc.*, 35th, 29-38, 1984.
- Davis, P. M., P. Slack, H. A. Dahlheim, W. V. Green, R. P. Meyer, U. Achauer, A. Glahn, and M. Granet, Teleseismic tomography of continental rift zones, in *Seismic Tomography: Theory and Practice*, edited by H. M. Iyer and H. Hirata, pp. 397-439, Chapman and Hall, New York, 1993.
- Deverchere, J., C. Petit, N. Gileva, N. Radziminovitch, V. Melnikova, and V. Sankov, Depth distribution of earthquakes in the Baikal rift system and its implications for the rheology of the lithosphere, *Geophys. J. Int.*, 146, 714-730, 2001.
- Diament, M., and M. G. Kogan, Longwavelength gravity anomalies and the deep structure of the Baikal rift, *Geophys. Res. Lett.*, 17, 1977-1980, 1990.
- Doser, D. I., Faulting within the western Baikal rift as characterized by earthquake studies, *Tectonophysics*, 196, 87-107, 1991.
- Dziewonski, A. M., and D. L. Anderson, Preliminary reference Earth model, *Phys. Earth Planet. Inter.*, 25, 297-356, 1981.
- Egorokin, A. V., S. K. Ziganov, and N. M. Chernyshev, The upper mantle of Siberia, *Proc. Int. Geol. Congr.*, 27th(8), 26-29, 1984.
- Engdahl, E. R., R. D. van der Hilst, and J. Berrocal, Imaging of subducted lithosphere beneath South America, *Geophys. Res. Lett.*, 22, 2317-2320, 1995.
- Fuchs, K., Seismic anisotropy and composition of the continental subcrustal lithosphere, *Proc. Int. Geol. Congr.*, 27th(8), 1-27, 1984.
- Gao, S., Seismic evidence for small-scale mantle convection under the Baikal rift zone, Siberia, Ph.D. thesis, 221 pp., Univ. of Calif., Los Angeles, 1995.
- Gao, S., P. M. Davis, H. Liu, P. D. Slack, Y. A. Zorin, V. V. Mordvinova, V. M. Kozhevnikov, and R. P. Meyer, Seismic anisotropy and mantle flow beneath the Baikal rift zone, *Nature*, 371, 149-151, 1994a.
- Gao, S., P. M. Davis, H. Liu, P. Slack, Y. A. Zorin, N. A. Logatchev, M. Kogan, P. Burkholder, and R. P. Meyer, Asymmetric upwarp of the asthenosphere beneath the Baikal rift zone, Siberia, *J. Geophys. Res.*, 99, 15,319-15,330, 1994b.
- Gao, S., P. M. Davis, H. Liu, P. D. Slack, A. W. Rigor, Y. A. Zorin, V. V. Mordvinova, V. M. Kozhevnikov, and N. A. Logatchev, *SKS* splitting beneath continental rift zones, *J. Geophys. Res.*, 102, 22,781-22,797, 1997.
- Gao, S., P. M. Davis, H. Liu, P. D. Slack, A. W. Rigor, Y. A. Zorin, V. V. Mordvinova, V. M. Kozhevnikov, and N. A. Logatchev, Reply to comment by A. Vauchez, G. Barruol, and A. Nicolas on "SKS splitting beneath continental rift zones", *J. Geophys. Res.*, 104, 10,791-10,794, 1999.
- Hess, H. H., Seismic anisotropy of the upper most mantle under oceans, *Nature*, 203, 629-631, 1964.
- Huismans, R. S., Y. Y. Podladchikov, and S. Cloetingh, Transition from passive to active rifting: Relative importance of asthenospheric doming and passive extension of the lithosphere, *J. Geophys. Res.*, 106, 11,271-11,291, 2001.
- Jackson, D. D., Interpretation of inaccurate, insufficient and inconsistent data, *Geophys. J. R. Astron. Soc.*, 28, 97-109, 1972.
- Jackson, D. D., and M. Matsu'ura, A Bayesian approach to nonlinear inversion, *J. Geophys. Res.*, 90, 581-591, 1985.
- Kaban, M. K., P. Schwintzer, and S. A. Tikhotsky, A global isostatic gravity model of the Earth, *Geophys. J. Int.*, 136, 519-536, 1999.
- Karato, S., Seismic anisotropy: Mechanisms and tectonic implications, in *Rheology of Solids and of the Earth*, edited by S. Karato and M. Toriumi, pp. 393-422, Oxford Univ. Press, New York, 1989.
- Kendall, J. M., Teleseismic arrivals at a mid-ocean ridge: Effects of mantle melt and anisotropy, *Geophys. Res. Lett.*, 21, 301-304, 1994.
- Kendall, J. M., and C. J. Thomson, Seismic modeling of subduction zones with inhomogeneity and anisotropy. 1. Teleseismic P-wavefront tracking, *Geophys. J. Int.*, 112, 39-66, 1993.
- Kennett, B. L. N., and E. R. Engdahl, Travel times for global earthquake location and phase identification, *Geophys. J. Int.*, 105, 429-465, 1991.
- King, S. D., and D. L. Anderson, An alternative mechanism of flood basalt formation, *Earth Planet. Sci. Lett.*, 136(3-4), 269-279, 1995.
- King, S. D., and D. L. Anderson, Edge-driven convection, *Earth Planet. Sci. Lett.*, 160(3-4), 289-296, 1998.
- Kiselev, A. I., Volcanism of the Baikal rift zone, *Tectonophysics*, 143, 235-244, 1987.
- Kiselev, A. I., and A. M. Popov, Asthenospheric diapir beneath the Baikal rift—Petrological constraints, *Tectonophysics*, 208, 287-295, 1992.
- Logatchev, N. A., and Y. A. Zorin, Baikal rift zone—Structure and geodynamics, *Tectonophysics*, 208, 273-286, 1992.
- Lysak, S. V., Terrestrial heat flow in the south of east Siberia, *Tectonophysics*, 103, 205-215, 1984.
- Lysak, S. V., Terrestrial heat flow of continental rifts, *Tectonophysics*, 143, 31-41, 1987.
- Montagner, J. P., and L. Guillot, Seismic anisotropy in the Earth's mantle, in *Progress in Geophysics for the New Millennium*, edited by E. Boschi, G. Ekstrom, and A. Morelli, pp. 217-253, Compositori, Bologna, Italy, 2000.
- Mordvinova, V. V., Method of the ratio of amplitude spectra of seismic vibrations as applied to studying the Baikal region, *Phys. Solid Earth*, 19, 887-893, 1983.
- Mordvinova, V. V., Spectra of seismic vibrations and lithospheric thickness in southern Siberia, *Phys. Solid Earth*, 24, 340-346, 1988.
- Parker, E. C., P. M. Davis, J. R. Evans, H. M. Iyer, and K. H. Olsen, Upwarp of anomalous asthenosphere beneath the Rio Grande rift, *Nature*, 312, 354-356, 1984.
- Petit, C., E. Burov, and J. Deverchere, On the structure and mechanical behavior of the extending lithosphere in the Baikal rift from gravity modeling, *Earth Planet. Sci. Lett.*, 149, 29-42, 1997.
- Petit, C., I. Koulakov, and J. Deverchere, Velocity structure around the Baikal rift zone from teleseismic and local earthquake travel-times and geodynamic implications, *Tectonophysics*, 296, 125-144, 1998.
- Popov, A. M., A deep geophysical study in the Baikal region, *Pure Appl. Geophys.*, 134, 575-587, 1990.
- Puzryev, N. N., *Detailed Seismic Studies of the Lithosphere by P- and S-Waves* (in Russian), 199 pp., Nauka, Novosibirsk, Russia, 1993.
- Puzryev, N. N., M. M. Mandelbaum, S. V. Krylov, B. P. Mishenkin, G. V. Petrik, and G. V. Krupskaya, Deep structure of the Baikal and other continental rift zones from seismic data, *Tectonophysics*, 45, 15-22, 1978.
- Ritsema, J., A. A. Nyblade, T. J. Owens, C. A. Langston, and J. C. Vandecar, Upper mantle seismic velocity structure beneath Tanzania, east Africa: Implications for the stability of cratonic lithosphere, *J. Geophys. Res.*, 103, 21,201-21,213, 1998.
- Ruppel, C., M. G. Kogan, and M. K. McNutt, Implications of new gravity data for Baikal rift zone structure, *Geophys. Res. Lett.*, 20, 1635-1638, 1993.
- Sherman, S. I., Faults and tectonic stresses of the Baikal rift zone, *Tectonophysics*, 208, 297-307, 1992.
- Silver, P. G., Seismic anisotropy beneath the continents—Probing the depths of geology, *Annu. Rev. Earth Planet. Sci.*, 24, 385-432, 1996.
- Silver, P. G., and W. W. Chan, Shear wave splitting and subcontinental mantle deformation, *J. Geophys. Res.*, 96, 16,429-16,454, 1991.
- Slack, P. D., P. M. Davis, H. A. Dahlheim, A. Glahn, J. R. Ritter, W. V. Green, P. K. H. Maguire, and R. P. Meyer, Attenuation and velocity of *P*-waves in the mantle beneath the East African rift, Kenya, *Tectonophysics*, 236, 331-358, 1994.
- Slack, P. D., P. M. Davis, W. S. Baldrige, K. H. Olsen, A. Glahn, U. Achauer, and W. Spence, The upper mantle structure of the central Rio Grande Rift region from teleseismic *P* and *S* wave travel time delays and attenuation, *J. Geophys. Res.*, 101, 16,003-16,023, 1996.
- Steckler, M. S., Uplift and extension at the Gulf of Suez: Indications of induced mantle convection, *Nature*, 317, 135-139, 1985.

928	Tapponnier, P., and P. Molnar, Active faulting and Cenozoic tectonics of the	Zorin, Y. A., and S. V. Osokina, Model of the transient temperature fields of	943
929	Tien Shan, Mongolia, and Baykal regions, <i>J. Geophys. Res.</i> , 84, 3425–	the Baikral rift lithosphere, <i>Tectonophysics</i> , 103, 193–204, 1984.	944
930	3459, 1979.	Zorin, Y. A., V. M. Kozhevnikov, M. R. Novoselova, and E. K. Turutanov,	945
931	Trampert, J., and H. J. van Heijst, Global azimuthal anisotropy in the	Thickness of the lithosphere beneath the Baikral rift zone and adjacent	946
932	transition zone, <i>Science</i> , 296, 1297–1299, 2002.	regions, <i>Tectonophysics</i> , 168, 327–337, 1989.	947
933	Turcotte, D. L., and S. H. Emerman, Mechanisms of active and passive		
934	rifting, <i>Tectonophysics</i> , 94, 39–50, 1983.		
935	Turcotte, D. L., and G. Schubert, <i>Geodynamics, Applications of Continuum</i>		
936	<i>Physics to Geological Problems</i> , John Wiley, New York, 1982.		
937	Zachary, J. A., K. H. Liu, and S. S. Gao, Rapid variation of crustal thick-	P. M. Davis and P. D. Slack, Department of Earth and Space Sciences,	949
938	ness from an ancient craton to a young orogenic belt, <i>Eos Trans. AGU</i> ,	University of California, Los Angeles, CA 90095, USA. (pdavis@ess.ucla.	950
939	81(48), Fall Meet. Suppl., Abstract S72A-30, 2000.	edu; pslack@linex.com)	951
940	Zorin, Y. A., and S. V. Lepina, Geothermal aspects of development of	S. S. Gao and K. H. Liu, Department of Geology, Kansas State	952
941	asthenospheric upwellings beneath continental rift zones, <i>J. Geodyn.</i> , 3,	University, Manhattan, KS 66506, USA. (sgao@ksu.edu; liu@ksu.edu)	953
942	1–22, 1985.	V. M. Kozhevnikov, V. V. Mordvinova, and Y. A. Zorin, Institute of the	954
		Earth's Crust, Siberian Branch of Russian Academy of Sciences, Irkutsk,	955
		Russia.	956

Article in Proof